Functionalized polysaccharides improve sensitivity of tyramide/peroxidase proximity labeling assays through electrostatic interactions

Malvina Heiniger,[1] Rosario Vanella,[1]* Zarah Walsh–Korb[1]* and Michael A. Nash[1,2]

[1] Department of Chemistry, University of Basel, Mattenstrasse 22, 4058 Basel, Switzerland
[2] Department of Biosystems Science and Engineering, ETH Zurich, Klingelbergstrasse 48, 4056 Basel, Switzerland

High-throughput assays that efficiently link genotype and phenotype with high fidelity are key to successful enzyme engineering campaigns. Among these assays, the tyramide/peroxidase proximity labeling method converts the product of an enzymatic reaction of a surface expressed enzyme to a highly reactive fluorescent radical, which labels the cell surface. In this context, maintaining the proximity of the readout reagents to the cell surface is crucial to prevent crosstalk and ensure that short-lived radical species react before diffusing away. Here we investigated improvements to tyramide/peroxidase proximity labeling for enzyme screening. We modified chitosan (Cs) chains with horseradish peroxidase (HRP), and evaluated the effects of these conjugates on the efficiency of proximity labeling reactions on yeast cells displaying D-amino acid oxidase. By tethering HRP to chitosan through different chemical approaches, we localized the auxiliary enzyme close to the cell surface and enhanced the sensitivity of tyramide/peroxidase labeling reactions. We found that immobilizing HRP onto chitosan through a 5 kDa PEG-linker improved labeling sensitivity by over 3.5-fold for substrates processed with low turnover rate (e.g., D-lysine), while the sensitivity of the labeling for high activity substrates (e.g., D-Alanine) was enhanced by over 0.6-fold. Such improvements in labeling efficiency broaden the range of enzymes and conditions that can be studied and screened with tyramide/peroxidase proximity labeling.

1 Introduction

A primary challenge in enzyme engineering is understanding the intricate relationships between the sequence, structure, and catalytic activity of enzymes. Strategies like directed evolution (DE)[1] and deep mutational scanning (DMS)[2,3] are regularly used to study and enhance catalytic enzymes for biomedical and industrial applications. However, the successful application of DE and DMS workflows to enzymes requires high-throughput screening methods that efficiently quantify the activity of many enzyme variants and link them with their respective genotype information at large scale.[4–6] If the enzymatic reaction cannot be easily linked with host cell survival (i.e., selection), a genotype-phenotype linkage may not be readily available. Consequently, substantial efforts have been made to customize high-throughput screening platforms for use with particular enzyme systems. In particular, scalable screening methods that can merge with next-generation DNA sequencing techniques are highly sought after.

Flow cytometry is a cornerstone of high-throughput screening, offering rapid and quantitative detection of cells expressing functional enzyme variants.[7] When enzyme variants are displayed on the cell surface, flow cytometry can efficiently detect immuno-labeled enzymes and quantify expression levels. Enzyme catalytic activity can also be measured through

proximity-based labeling protocols that detect catalytic phenotypes at high-throughput. This process ensures the preservation of the genotype-phenotype linkage, crucial for recovering genetic information responsible for the change in the activity of the studied catalyst.[4] Traditionally, screening relied on multiwell plates, which limited analysis to one variant population per well, resulting in laborious and time-consuming processes, especially when dealing with large variant libraries. More recently, microfluidic platforms have further streamlined cell compartmentalization and high throughput screening at the single-cell level.[8] This has been achieved by employing droplet encapsulation techniques, allowing for a substantial increase in throughput.[5,9,10] However, these platforms often come with a significant cost and demand specialized expertise for construction and operation. The ideal scenario is a system where the cell itself acts as a compartment, where single cell activity assays are used to label specific cells in bulk with high fidelity. This concept presents a more streamlined approach to single-cell analysis. The challenge here lies in specific cell labeling methods that link genotype and phenotype with high fidelity. Recent advances in labeling strategies include nanoparticle labeling,[11] affinity screening,[12] and proximity labelling.[13,14]

We are particularly interested in developing high-throughput screening methods for enzyme activities based on proximity labeling.[6,15–17] These methods link enzymatic activity, either directly or through reaction cascades, to the production of highly reactive and fluorescent phenoxyl radical species, which are utilized for labeling purposes. Commonly, an oxidoreductase, such as horseradish peroxidase (HRP), engineered ascorbic acid peroxidase (APEX2),[18,19] laccase,[20] or tyrosinase,[21] is introduced into the labeling reaction to produce the phenoxyl radical by reaction with the by-products of the main enzymatic reaction at the cell surface, after the addition of an enzyme-specific substrate (Figure 1A). The dye-labeled phenoxyl radical then covalently binds to the cell surface through tyrosine moieties, permitting detection. This approach has been highly successful in the screening of enzyme variant libraries.[22] Enzyme variants under investigation are presented on the surface of host cells, making them easily accessible for detection and testing without additional sample manipulation. When the reaction substrate is added, each enzyme variant converts the substrate into the product, staining the cell surface. The cellular pool can then be sorted based on the intensity of the fluorescent tyramide label to enrich variants of interest carrying mutations that enhance the labeling efficiency and, therefore, reactivity of the enzyme. However, one challenge in such a system is that the products of the primary enzymatic reaction can diffuse away from the cell surface before reacting with the readout components (Figure 1B). Thus, maintaining proximity of the reactants to the site of the primary enzymatic reaction is critical to prevent non-specific staining of nearby cells and preserve screening fidelity (Figure 1C).

We have previously investigated strategies and improvements to the tyramide labeling assay applied for high-throughput screening of D-amino acid oxidase variants displayed on the surface of yeast cells. Prior work from our lab showed that maintaining a low cell density (~50,000 cells/100 µl) in suspension and using high concentrations of the auxiliary enzyme HRP were necessary to confine the activated fluorescent tyramide molecules to the cell surface and prevent non-specific staining of neighboring cells expressing other variants.[18] In the present work, by employing chitosan (Cs), an easily functionalized aminated polysaccharide,[23] we aimed at enhancing the localization of HRP in close proximity to the yeast cells, controlling crosstalk signals and improving screening efficiency by coupling HRP to Cs. We explored how electrostatic interactions between positively charged HRP-Cs and

the negatively charged cell surface could enhance proximity. We present different HRP-Cs conjugation methods and report the outcomes of proximity labeling using the tyramide assay to screen D-amino acid oxidase on a variety of substrates catalyzed at different velocities by the enzyme (from high to low turnover rate).

D-amino acid oxidase from the yeast *Rhodotorula gracilis* (RgDAOx) is an ideal model system for such investigations. It possesses high substrate promiscuity towards a wide range of D-amino acids with differing levels of activity.[24–26] RgDAOx has a clear order of substrate preference, with non–polar substrates (e.g., D–Ala, D–Leu, D–Val) being favored (high turnover rate substrates), followed by aromatics (D–Trp), and more hydrophobic (e.g., D–Ser and D–Pro) substrates. Positively charged amino acids (D–His, D–Arg and D–Lys) are turned over poorly, while no or low activity is detectable with negatively charged amino acids (D–Asp and D–Glu).[25,27] The broad substrate scope and the differing levels of activity offered a means to assess the efficiency of HRP-functionalized Cs to promote efficient cell labeling and assaying in a high throughput manner when coupled with flow cytometry.

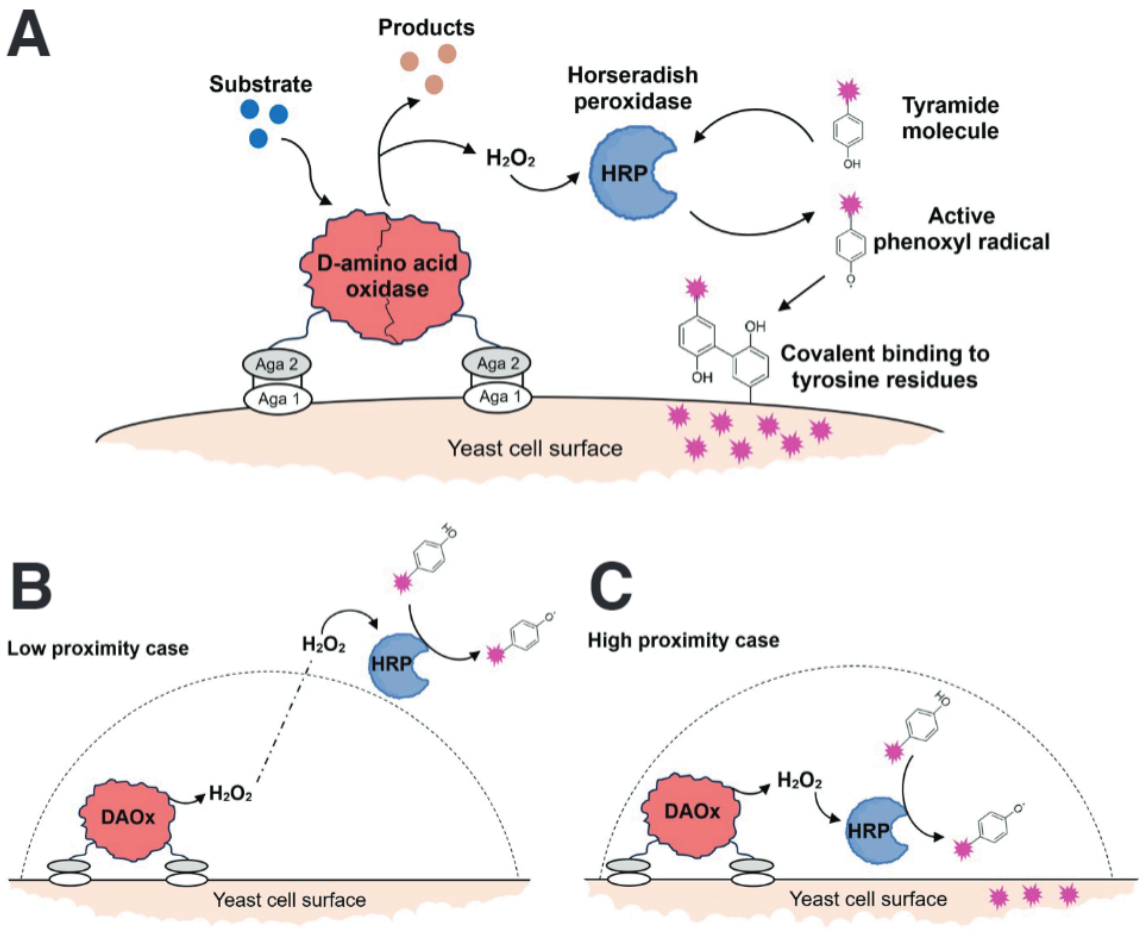

Figure 1: Graphical illustration of (A) the tyramide-peroxidase proximity labeling assay with *Rg*DAOx as the model enzyme expressed on the surface of a yeast cell. (B) The low proximity labeling scenario where the formation of phenoxyl radical occurs far from the cell surface, resulting in diffusion away from the cell surface of the radical species. (C) The high proximity labeling scenario where the reaction cascade begins and ends in the vicinity of the cell surface, thus enabling efficient labeling of the cell expressing the studied enzyme.

Our approach involves the coupling (physical or covalent) of HRP onto chitosan chains of varying length, which, through charge directed encapsulation, maintains the close proximity of the HRP to the cell surface to enhance the outcome of tyramide/peroxide proximity labeling reactions. The following sections detail the optimization of the coupling approach, comparing physically immobilized HRP bioconjugates with covalently coupled (through carboxyl or cysteine residues), the subsequent evaluation of cell encapsulation and labeling as a function of coupling approach and the application of the method to evaluate how targeted proximity labeling can improve labeling efficiency for low turnover rate substrates.

2 Experimental

2.1 Materials

With the exception of Amplex Red (Cayman, MI, USA), primary and secondary antibodies, Cs (M_w = ca. 150 kDa), (Thermo Fisher Scientific, Basel, CH) and functionalized polyethylene glycol (PEG) linkers (Rapp Polymere GmbH, Tübingen, DE), all reagents were purchased from Sigma Aldrich Chemie GmbH (Buchs, CH). Ultrapure water was obtained from an in house Milli-Q water purification system (Millipore, MA, USA) and is denoted as MQ water throughout the text.

2.2 Instrumentation

Labeling efficiency was determined by cell screening on an Attune NxT flow cytometer (Thermo Scientific) equipped with 488 nm and 561 nm lasers. Data analysis was carried out using Attune NxT software v.3.2.1 (Life Technologies). Cell populations of interest were separated through gating. Measurements were performed in triplicate and 10,000 cells were recorded and analyzed per sample.

The activity of the *Rg*DAOx with the substrates of interest was determined using an Amplex Red fluorescence assay. Fluorescence spectra were measured with a TECAN Safire 2 Multi Detection Plate Reader using non-transparent 96 well plates (Thermo Fisher Scientific). Amplex Red assays for H_2O_2 production were measured with a gain of 50 and Z-position of 13.2 mm. Fluorescence at 590 nm was recorded every 120 s for a total of 30 cycles with a shake duration between cycles of 10 s at 37°C. All measurements were performed in triplicate.

Verification of the functionalization of Cs with HRP was done using mass photometry on a Refeyn One MP Mass Photometer equipped with AcquireMP data analysis software. Samples were prepared by dissolving the material to give a stock concentration of 0.5 mg/ml. Samples were further diluted until a final concentration between 5 - 50 nM was achieved. Thyroglobulin (monomer (Mw = 330 kDa) and β-Amylase (monomer (58 kDa), dimer (Mw = 116 kDa), tetramer (Mw = 233 kDa)) were used as the mass standards for the measurements. The estimated mass of the constructs was deduced from the average of at least 10,000 interactions (adsorption and desorption) of the molecules of interest at the glass slide interface over a period of 120 s.

2.3 Methods

2.3.1 Expression and surface display of wild type *Rg*DAOx

*Rg*DAOx positive colonies were obtained as described by Vanella, *et al.*[22] Yeast colonies were pre-cultured in -TRP liquid medium with 2 wt.% glucose for 24 h at 30°C to an OD_{600} = 8 with continuous shaking at 224 *g* in an incubator/shaker (Innova 44, New Brunswick Scientific, NJ, USA). Protein expression and display were induced by transferring the culture at a starting OD_{600} = 0.4 to fresh liquid medium containing 0.2 wt.% glucose, 1.8 wt.% galactose and 100 mM citrate/phosphate buffer (pH 7) to facilitate the best expression conditions. Yeast cells were expressed at 20°C under continuous shaking (224 *g*) for 48 h, before being pelleted by centrifugation at 3920 *g* for 4 min (5920 R, Eppendorf, NJ, USA). Cells were washed with PBS containing 0.1 wt.% bovine serum albumin (PBS/BSA), re-suspended in 1 ml of the same buffer and stored at 4°C until required.

2.3.2 Antibody staining for surface displayed *Rg*DAOx

After display, yeast cells were washed twice with PBS/BSA before being re-suspended at a concentration of 21,000 cells/µl in the same buffer. These cells were incubated at room temperature (RT) for 30 min with 2 µg/ml primary anti-6x-His mouse monoclonal antibody. After incubation, cells were washed twice with cold PBS/BSA and re-suspended at the same concentration in 1 ml of cold buffer containing 4 µg/ml of secondary goat anti-mouse antibody conjugated with Alexa Fluor 594. Cells were incubated at 4°C for 30 min, washed twice with cold PBS/BSA and re-suspended to achieve a final cell concentration of 100,000 cells/µl. Surface expression of *Rg*DAOx was confirmed by flow cytometry.

2.3.3 Biotinylation of chitosan with biotin-PEG-NHS linker

Biotinylated chitosan (biot-Cs) was prepared by dissolving 20 mg Cs (M_w = 60 kDa) in 1 ml 1 vol.% AcOH (2 wt.%, 0.38 mM). Biotin-PEG-NHS (46.4 mg, M_w = 5,359 Da, 8.66 mM) at a ratio of 26:1 of Biotin-PEG-NHS:Cs was added to 1 ml of HEPES buffer (0.1 M) (pH 7.5). Upon dissolution, 1 ml of the 2 wt.% Cs soln. was added to give a final concentration of 10 mg/ml (1 wt.%) and stirred at RT for 2 h. The reaction mixture was transferred to a dialysis bag with a molecular weight cut-off (MWCO) of 50 kDa, then dialyzed against MQ water (5 L) for 24 h. Water was exchanged and dialysis continued for a further 24 h. The dialyzed reaction mixture was collected in a Falcon tube and stored at -80°C for 24 h. The frozen reaction mixture was lyophilized (-54°C, 56 mbar) until solid (24 h). From the weight of the dry product and reagents, a functional density of 2.2% was estimated. Biot-Cs was dissolved in acetate buffer (pH 6) to give a 1.5 wt.% stock soln. for further use.

2.3.4 Functionalization of Cs with HRP (carboxyl coupling)

HRP-functionalized Cs (HRP-Cs) was synthesized using aqueous phase carbodiimide chemistry. Solutions of different molecular weights of Cs (M_w = ca. 60 kDa, and ca. 150 kDa) were prepared by dissolving 20 mg of each Cs in a 1 vol.% AcOH to give a final concentration of 2 wt.% (0.38 mM or 0.13 mM, respectively). Subsequently, HRP (29.3 mg, M_w = 44 kDa, 0.66 mM) was added to 1 ml MQ water. Upon dissolution of the HRP, *N*-hydroxysuccinimide (NHS, 0.15 mg, M_w = 115 Da, 1.3 mM) and *N*-(3-dimethylaminopropyl)-*N*-ethylcarbodiimide (EDC, 0.25 mg, M_w = 192 Da, 1.3 mM) were added and stirred at RT for 1 h. From the desired 2 wt.% Cs soln., 1 ml was added to the

reaction mixture to give a final concentration of 1 wt.% and stirred at RT for 16 h. After functionalization, the reaction mixture was transferred to a dialysis bag with MWCO = 50 kDa for the HRP-Cs (60 kDa) and MWCO = 100 kDa for the HRP-Cs (150 kDa) constructs. All were dialyzed against MQ water (5 L) for 48 h. Water was exchanged and dialysis continued for a further 24 h. The reaction mixture was collected from the dialysis membrane into a syringe before being filtered with a PTFE SYR 0.45 µm 25 mm filter due to heavy precipitation. The filtered mixture was collected in a Falcon tube and stored at -80°C for 24 h and then lyophilized (-54°C, 56 mbar) until solid, to yield HRP-Cs60 and HRP-Cs150. All HRP-Cs were dissolved in acetate buffer (pH 6) to give a 1.6 wt.% stock soln. for further use. The molecular weight was checked with mass photometry to ensure that the HRP-Cs was the main product of the reaction, see Supplementary Figure S1A, S1BB and Supplementary Figure S2A and S2B.

Table 1: Detailed composition of each of the labeling reaction tests, where the substrate in each case was D-Ala

biotinylated-Cs								
Construct	***Rg*DaOX cells 100,000 cells/µl**	**Tyramide 1/100 dilution**	**HRP 9 mM**	**st-HRP 0.012 mM**	**biot-Cs 1.5 wt.%**	**Cs 1.5 wt.%**	**Substrate 100 mM**	**Buffer PBS/BSA**
st-HRP+biot-Cs	1 µl	5 µl	–	8.32 µl	33 µl	–	35 µl	17.68 µl
HRP+biot-Cs	1 µl	5 µl	0.5 µl	–	33 µl	–	35 µl	25.5 µl
st-HRP+Cs	1 µl	5 µl	–	8.32 µl	–	33 µl	35 µl	17.68 µl
HRP+Cs	1 µl	5 µl	0.5 µl	–	–	33 µl	35 µl	25.5 µl
HRP	1 µl	5 µl	0.5 µl	–	–	–	35 µl	58.5 µl
HRP-Cs/HRP-PEG-Cs								
Construct	***Rg*DaOX cells 100,000 cells/µl**	**Tyramide 1/100 dilution**	**HRP 0.9 mM**	**HRP-Cs 1.6 wt.%**	**HRP-PEG-Cs 1.6 wt.%**	**Cs 1.6 wt.%**	**Substrate 100 mM**	**Buffer PBS/BSA**
HRP-Cs	1 µl	5 µl	–	30.93 µl	–	–	35 µl	28.07 µl
HRP-PEG-Cs	1 µl	5 µl	–	–	30.93 µl	–	35 µl	28.07 µl
HRP+Cs (150 kDa)	1 µl	5 µl	4.95 µl	–	–	30.93 µl	35 µl	23.12 µl
HRP	1 µl	5 µl	4.95 µl	–	–	–	35 µl	54.05 µl

2.3.5 Functionalization of Cs with HRP through malhex-PEG-COOH linker (Cysteine coupling)

To increase the freedom of movement of the HRP, a 5 kDa PEG spacer was inserted between the HRP and Cs using thiol-maleimide click chemistry and aqueous phase carbodiimide chemistry to give HRP-PEG-Cs. Solutions of Cs (ca. 60 kDa and 150 kDa) were prepared as above. Subsequently, HRP (29.3 mg, M_w = 44 kDa, 0.66 mM) and malhex-PEG-COOH (3.49 mg, M_w = 5,241 Da, 0.66 mM) were added to 1 ml PBS and stirred at RT for 1 h. Afterwards, NHS and EDC were added in excess (2-fold, as in Section 2.3.4) and stirred at RT for 1 h. 1 ml of the desired 2 wt.% Cs soln. was added to the reaction mixture to give a final concentration of 1 wt.% and stirred at RT for 16 h. Dialysis and lyophilization were carried out as per Section 2.3.4. HRP-PEG-functionalized chitosan (HRP-PEG-Cs60 or HRP-PEG-150) was dissolved in acetate buffer (pH 6) to give a 1.6 wt.% stock soln. for further use. The molecular weight was checked with mass photometry (Supplementary Figure S1A and S1C and Supplementary Figure S2A and S2C) to ensure that the HRP-PEG-Cs was the main product of the reaction.

2.3.6 Tyramide/peroxidase proximity labeling assay

2.3.6.1 Labeling assay with biotinylated chitosan and st-HRP

Master mixes (100 µl) were prepared for each of the HRP-Cs constructs as outlined in Table 1. To accurately evaluate the effect of the interaction between the st-HRP and biot-Cs bioconjugate, four controls were performed in which st-HRP was replaced with HRP (HRP+biot-Cs), biot-Cs was replaced with unfunctionalized Cs (st-HRP+Cs, Cs stock conc. 1.5 wt.%), both st-HRP and biot-Cs were replaced (HRP+Cs) and finally, one reaction with HRP and no chitosan. All experiments were incubated for 60 min at RT. After incubation, the reaction mixture was diluted with 400 µl of PBS/0.1 wt.% BSA. The yeast cells were recovered through centrifugation (14,000 *g*, 30°C, 2.5 min), washed twice with PBS/0.5 vol.% AcOH (pH 5) and once with PBS/0.1 wt.% BSA/0.05 wt.% TWEEN20 and re-suspended in 250 µl of PBS/BSA. All reactions were carried out in triplicate and labeling efficiency assessed by flow cytometry.

2.3.6.2 Labeling assay with HRP-Cs and HRP-PEG-Cs

Master mixes (100 µl) were again prepared as in Section 2.3.6.1, with HRP-Cs and HRP-PEG-Cs replacing both free st-HRP and biot-Cs, see Table 1. Both were added to the master mix to achieve 0.5 wt.% polymer in the reaction mixture. The substrate was added last. In the optimization phase only D-Ala and D-Lys were used as the substrates, representing high (D-Ala) and low (D-Lys) turnover rate substrates. For the study of substrate variation, D-Leu, D-Ser, D-Val, D-Trp, D-Pro, D-His, and D-Arg were also used, see Table 2. Work-up and analysis were conducted as per Section 2.3.6.1. To verify that tethering the HRP to Cs was necessary for enhancing proximity labeling, controls were performed in which HRP-Cs or HRP-PEG-Cs were replaced with free HRP and unfunctionalized Cs. For these experiments, 150 kDa unfunctionalized Cs were tested individually, to see if any observed differences were related to chain length. From a stock concentration of 1.6 wt.%, Cs was added to the reaction to achieve a solid content of 0.5 wt.%, while HRP was added to achieve a final concentration of 45 µM, as per Table 1. A final control was conducted in which 20 wt.% PEG (M_w = 3350 Da) was added to observe if

increasing the viscosity would further improve the proximity labeling. In this case, the standard conditions for the HRP-PEG-Cs (Table 1) were used with 20 µl of the buffer replaced with PEG3350. The rest of the procedure was followed as Section 2.3.6.1.

2.3.7 Amplex Red activity assays

2.3.7.1 Comparison of the catalytic activity of HRP *vs.* HRP/Cs constructs

The catalytic activity of HRP and HRP-PEG-Cs were compared using an Amplex Red activity assay. Multiple concentrations of free HRP (40 µM, 45 µM, 50 µM) were tested against st-HRP, HRP-Cs and HRP-PEG-Cs, at the concentrations selected for the labeling reactions, 1 µM, 0.5 wt.% and 0.5 wt.%, respectively. For these stock solutions (100 µl), the volume of the buffer was adjusted from 94.5-95.6 µl to account for decreasing/increasing the HRP stock volume in the master mix (from 4.4-5.5 µl). In a black bottom 96-well plate, 50 µl of a master mix (100 µl) containing 10 µl of a diluted (1/100) HRP stock solution, 0.5 µl of a 38.8 mM stock solution of Amplex Red in DMSO (194 µM) and 89.5 µl PBS were added. Identical master mixes were prepared in which HRP was replaced with st-HRP+biot-Cs, HRP-Cs or HRP-PEG-Cs. Before measuring fluorescence, 50 µl 1 mM H_2O_2 (0.5 mM) was added using a multi-channel pipette. After adding H_2O_2 to the enzyme reaction mixture, the plate was loaded on the plate reader and fluorescence at 590 nm was recorded every 15 s for a total of 60 cycles. Fluorescence for each time point was measured in duplicate.

2.3.7.1.1 Comparison of the catalytic activity of *Rg*DAOx as a function of substrate

The activity of *Rg*DAOx on several D-amino acid substrates, listed in Table 2, was determined by Amplex Red activity assays. In a black bottom 96-well plate, two master mixes with a combined total volume of 100 µl were prepared. Master mix 1 contained 1 µl of a 100,000 cells/µl soln. of yeast cells in PBS/BSA (100 k/100 µl) and was made up to 59.1 µl in the same buffer before transferring to the wells of the plate. Master Mix 2 contained 4.95 µl of an 0.9 mM soln. of HRP (45 µM), between 1.8 and 70 mM of substrate (see Table 2), 1 µl of a 38.8 µM soln. of Amplex red (388 µM), in a final volume of 40.9 µl made up with PBS/BSA. Master Mix 2 was quickly added to the first master mix in the wells using a multi-channel pipette. The plate was loaded on the plate reader and fluorescence at 590 nm was recorded every 120 s for a total of 30 cycles. Fluorescence for each condition was measured in triplicate.

Table 2: Substrates and concentrations used for both tyramide labeling assays (Section 2.3.6.1) and Amplex Red activity assays

Substrate	**Conc. mg/ml**	**Stock soln. mM**	**Reaction conc. mM**
D-Ala	9	100	35
D-Leu	13	100	35
D-Val	24	200	70
D-Ser	17	160	57
D-Trp	1	5	1.8
D-Pro	24	200	70
D-Lys	28	200	70
D-His	30	200	70
D-Arg	34	200	70

3. Results and Discussion

3.1 Immobilization of HRP on chitosan using physical and covalent linkages

Previous work from our group on the *Rg*DAOx enzyme displayed on the yeast surface found that the sensitivity and fidelity of peroxidase/tyramide proximity labeling reactions could be enhanced by saturating the labeling reaction mixture with the auxiliary enzyme HRP and/or by the addition of viscous polymers (i.e., 20 wt.% poly(ethylene glycol) into the reaction mixture to slow the diffusion of reagents and maintain reagent proximity to the cell surface.[6,16,22] However, even at HRP concentrations up to 250 μM in highly viscous mixtures, we observed that when testing *Rg*DAOx using substrates processed at low catalytic rate we could not accurately assay the reaction using the peroxidase/tyramide proximity cell labeling method because substrate turnover was simply too slow, and diffusive processes led to loss of specific signal.[28] We hypothesized that if the HRP was localized at the cell surface by tethering to a polymer chain with an electrostatic affinity for the cell surface, we could keep the HRP close to the cell for the duration of the labeling reaction without the need for high HRP concentrations or viscosity modifiers. We focused on three tethering strategies to test this hypothesis: (1) bioconjugation of streptavidin-HRP (st-HRP) to biotin functionalized chitosan (biot-Cs) (Figure 2A), (2) direct conjugation of HRP to Cs through carboxyl coupling (Figure 2B) and (3) conjugation of the HRP to Cs through a PEG spacer using cysteine coupling (Figure 2C).

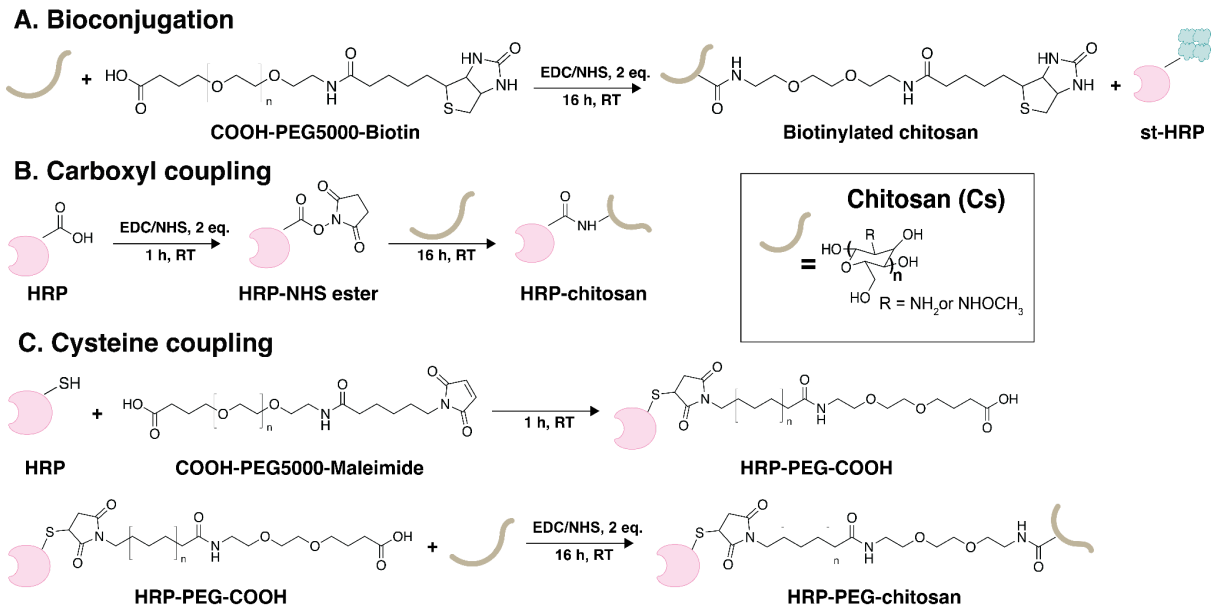

Figure 2: Graphical representation and schematics of the chitosan HRP conjugation approaches: (A) st-HRP bioconjugate bound to biotinylated chitosan, (B) conjugation of HRP to chitosan through an available carboxyl group using carbodiimide chemistry, (C) conjugation of HRP to chitosan through an available thiol group from a cysteine residue using thiol-maleimide click chemistry and a PEG linker.

The bioconjugation approach exploits the well-known biotin-streptavidin interaction to physically complex a commercially available st-HRP to biot-Cs, thus, physically immobilizing it on the chitosan chain. The functionalization with biotin was carried out using a biotinylated PEG chain of 5 kDa that also possessed a terminal carboxyl group to permit binding to the Cs chain using carbodiimide coupling with EDC/NHS (Figure 2A). Using a mass-based approximation, i.e., comparing the weight of the unfunctionalized Cs with that of the biotinylated Cs after washing, we estimated a biotinylation density of 2.2% on the 60 kDa Cs chain. This corresponded to ~5.87 amine groups modified with biotin per chitosan chain. The Cs monomer length has been reported as 0.52 nm, thus the 60 kDa chain used here is estimated at ~138 nm in length.[29] Based on a molecular weight of 100 kDa and an hydrodynamic diameter (D_H) of ~13 nm (5 nm for streptavidin and 8 nm for HRP)[30,31] for the st-HRP conjugate, we estimate that ~6 st-HRP conjugates could be immobilized on the chitosan chain. We first conjugated biot-Cs with 1 µM st-HRP, which corresponds to a functional density of approximately 1.2 % with respect to the number of available biotins per chitosan chain. To establish an appropriate negative control for the tyramide reaction, we subsequently assessed the performance of st-HRP compared to soluble free HRP using an Amplex Red activity assay (Supplementary Figure S3). The assay revealed that the activity of unconjugated 1 µM st-HRP was comparable to that of 45 µM free HRP, likely attributable to the superior purity of the st-HRP in comparison to commercially available free HRP. Therefore, in subsequent experiments utilizing st-HRP+biot-Cs, we compared the performance of immobilized HRP to that of 45 µM total free HRP in the control experiment.

In parallel we evaluated covalent coupling of HRP to Cs chains of varying chain lengths, either through carboxyl groups using carbodiimide chemistry or through cysteine residues using heterobifunctional PEG spacers (Figure 2B and C). Given the length of the chitosan chains available (60 and 150 kDa) and the size of the HRP (44 kDa), we aimed for 1 HRP per chain for all chain lengths. This was done for both the carboxyl and cysteine coupling

approaches. Successful conjugation of HRP to Cs using both coupling approaches was confirmed by mass photometry (Supplementary Figure S1 and S2). We chose these two different coupling approaches to understand if the carbodiimide chemistry provided a more random functionalization approach with less reproducibility compared to cysteine coupling, which, given that there are only 8 cysteine residues in HRP, should be more specific. We also reasoned that the inclusion of a 5 kDa PEG spacer would improve the accessibility of the bound HRP.

For the carboxyl coupling, the HRP was first mixed with the NHS/EDC to prime the COOH groups for reaction with the amines of the Cs, and then mixed with the Cs of the desired Mw. For the cysteine coupling, we modified the thiol groups of the cysteines on HRP with a maleimide-PEG5000-COOH linker, providing us with a PEGylated-HRP that reacted with Cs in the presence of NHS/EDC. Notably, the 8 Cys moieties reported in the HRP sequence all form disulfide bonds (Cys11:Cys91, Cys44:Cys49, Cys97:Cys301 and Cys177:Cys209).[32] However, analysis of the accessible surface area (ASA) using the Protein Data Bank's electronic Proteins, Interfaces, Structures and Assemblies tool (PDBePISA) showed that Cys91 is very accessible to solvent, with an ASA of approximately 14.2 $Å^2$.[33–35] All other Cys residues had an ASA of 2.8 $Å^2$ or less. Furthermore, analysis of disulfide bond strain energy using the formula derived by Katz and Kossiakoff, indicated that the Cys11:Cys91 and the Cys44:Cys49 would be the easiest to cleave given their high dihedral strain energy.[36] Given the low accessibility of the Cys44:Cys49 and its proximity to the active site of the HRP, this was an unlikely target for cleavage. We hypothesized that in the presence of chitosan, a mild reducing agent,[37–39] it would be possible to cleave the disulfide bond between the Cys11:Cys91 leaving the Cys91 exposed to bind to chitosan. We relied on thiol-maleimide click chemistry due to the relatively mild reaction conditions, the fact that no further modification of the protein is required other than disulfide bond cleavage, and no heavy metals are introduced into the system.[40] Given the more exposed nature of the PEG-COOH after reaction with the HRP, compared to the COOH groups of the protein, the preference should be for the linkage to occur through the PEG chain, rather than the HRP being attached at any other point on its surface.

Mass photometry, also known as interferometric scattering microscopy, was used to assess the success of the functionalization approaches. This is a particularly useful technique for the molecular weight determination of macromolecules, which due to size, composition or charge, are difficult to analyze through standard mass determination techniques, such as NMR, mass spectrometry or size exclusion chromatography.[41–43] For the 60 kDa chitosan, a straightforward transition was observed from 64 kDa before functionalization to 108 kDa after HRP-functionalization and 117 kDa after HRP-PEG-functionalization (Supplementary Figure S1), essentially indicating that each Cs chain has 1 HRP or, when the 5 kDa PEG is introduced, 1 HRP and 1 PEG spacer. Interpretation of the 150 kDa functionalization is less clear due to the cleavage of the 150 kDa chitosan chains during the first step of the functionalization, the NHS/EDC coupling step. We observed that the molecular weight of the functionalized 150 kDa Cs was unusually low after addition of the HRP or HRP-PEG. To understand this reduction in Mw, we performed the reaction of the 150 kDa Cs with NHS/EDC without the addition of HRP or HRP-PEG. This showed that the approximately 150 kDa chains were cleaved to approximately 105 kDa in 1 h of reaction (Supplementary Figure S2A and S2B). After addition of just HRP this cleavage likely continued resulting in a Mw of the unfunctionalized of approx. 67 kDa and the functionalized Cs of 119 kDa, which

once again indicates 1 HRP per chain but little difference between the final molecular weight of the HRP-Cs60 and the HRP-Cs150. When the PEG spacer is introduced the variation in molecular weights is more extensive and fitting is difficult but there appears to be 3 Mw distributions, centered at approximately 85 kDa, 125 kDa and 185 kDa, indicating the presence of unfunctionalized chains, 1xHRP-PEG per chain and possibly also 2xHRP-PEG units per chain.

3.2 Effect of HRP immobilization strategy on cell labeling efficiency

After preparation of the three chitosan constructs, the physically immobilized bioconjugate, the carboxyl coupled HRP and the cysteine coupled HRP conjugates, we assayed the effect of these constructs on tyramide labeling efficiency using yeast cells displaying the wild type *Rg*DAOx and two reference substrates transformed by the enzyme at high (D-Ala) and low (D-Lys) reaction velocities. In each case antibody-stained *Rg*DAOx displaying cells were incubated with the st-HRP/biot-Cs bioconjugate (Figure 3A and 3D), the HRP-Cs (Figure 3B and 3E) or the HRP-PEG-Cs (Figure 3C and 3F) in the presence of fluorophore-labeled tyramide and the amino acid substrate (D-Ala (Figure 3A, 3B and 3C) or D-Lys (Figure 3D, 3E and 3F)) for 1 h. Following incubation, samples were washed and analyzed by flow cytometry. Before tyramide-labeling, the antibody-stained cells were visible in the top left quadrant (+/-), with the bottom left quadrant (-/-) showing cells that remain unstained because they did not express *Rg*DAOx. We determined the success of the tyramide labeling strategy by quantifying the shift of the cell populations from the +/- gate (white quadrant, Figure 3) to the +/+ gate, (green quadrant, Figure 3), indicating cells that have been both antibody-stained and tyramide labeled, referred to as the +/+ population. The relative shifts were compared to those observed when free HRP was used in the labeling reaction instead of one of the designed polymeric constructs, to determine improvements introduced by the constructs over the state-of-the-art. As we can only label what has been expressed we report the changes as a percentage of the total expressing cell population (+/- and +/+).

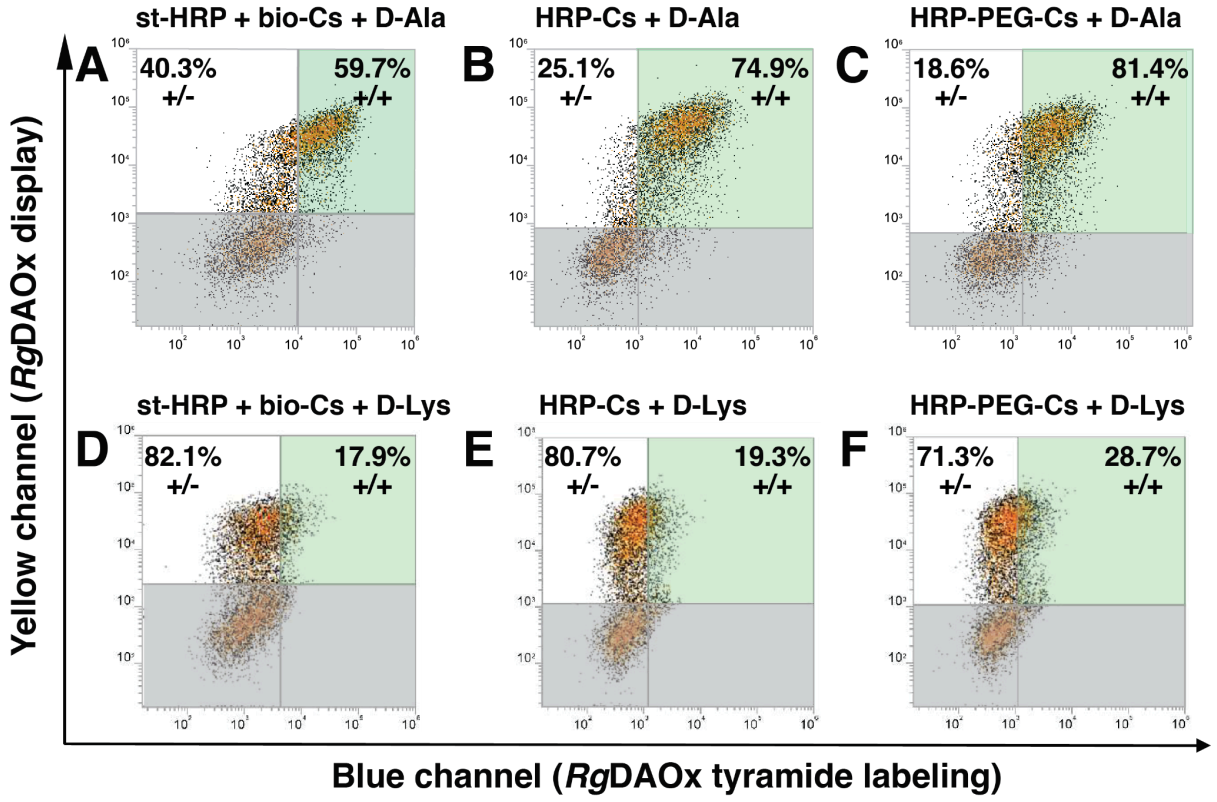

Figure 3: Flow cytometry plots showing population shift (%) from the +/- gate (in white) to the +/+ gate (in green) after the tyramide labeling assay, as a function of construct and substrate for (A) st-HRP+biot-Cs with D-Ala, (B) HRP-Cs150 with D-Ala, (C) HRP-PEG-Cs150 with D-Ala, (D) st-HRP+biot-Cs with D-Lys, (E) HRP-Cs150 with D-Lys, (F) HRP-PEG-Cs150 with D-Lys. Gray boxes highlight the unlabeled/unstained cells not used for the calculation of efficiency, in all cases n=3.

3.2.1 st-HRP bioconjugation to chitosan

Despite the low functionalization achieved with the physically immobilized HRP bioconjugate, an increase in labeling percentage of the yeast population was observed for both the D-Ala and D-Lys substrates (Figure 4A,i and 4B,i). Figure 4A shows the percentage population shift in the +/+ gate for the experiment performed with st-HRP+biot-Cs bioconjugate reaching a value of just under 60%. Figure 4B shows results of the same experiment performed using a low activity substrate (D-Lys), where we registered a labeling efficiency of ~18%. We compared the outcome of the reactions performed with st-HRP bioconjugate alongside relevant controls for both D-Ala and D-Lys substrates. The presence in the labeling reaction of 45 μM free HRP induced a shift of ~52% of the yeast population for D-Ala, 8% lower than the shift induced by the bioconjugate. In the case of D-Lys, the free HRP induced a shift of just 6% of the population, 12% lower with respect to the reaction with the bioconjugate. Further controls that replaced st-HRP or biot-Cs in the complex with free HRP, free Cs or both, confirmed that formation of the st-HRP+biot-Cs complex was required to produce improvements in labeling efficiency when either D-Ala (Figure 4A) or D-Lys (Figure 4B) were used as substrates. Furthermore, increasing the concentration of free HRP higher than 45 μM (Supplementary Figures S5 and S6) didn't significantly increase the cell fraction found in the +/+ gate. This validated our hypothesis that it was not necessary to saturate the system with HRP, if HRP is effectively targeted to the cell surface through Cs charge interactions. However, we did observe also an increase in labeling efficiency

compared to the free HRP experiment, when using the st-HRP (no biot-Cs) with the D-Ala substrate (Figure 4A,iii) almost to the same extent as for the st-HRP+biot-Cs bioconjugate (Figure 4A,i). This effect was not as pronounced with D-Lys, and is likely related to interactions between the mannosylated yeast surface and the streptavidin of the conjugate. Previous reports showed that sugars, in particular mannose, can hinder streptavidin-biotin binding through interactions with the biotin binding pocket of streptavidin.[44,45] As the labeling efficiency of the st-HRP experiment is similar to that of the conjugate, and only in the case of the high activity substrate, the complex still produces the most favorable effects overall.

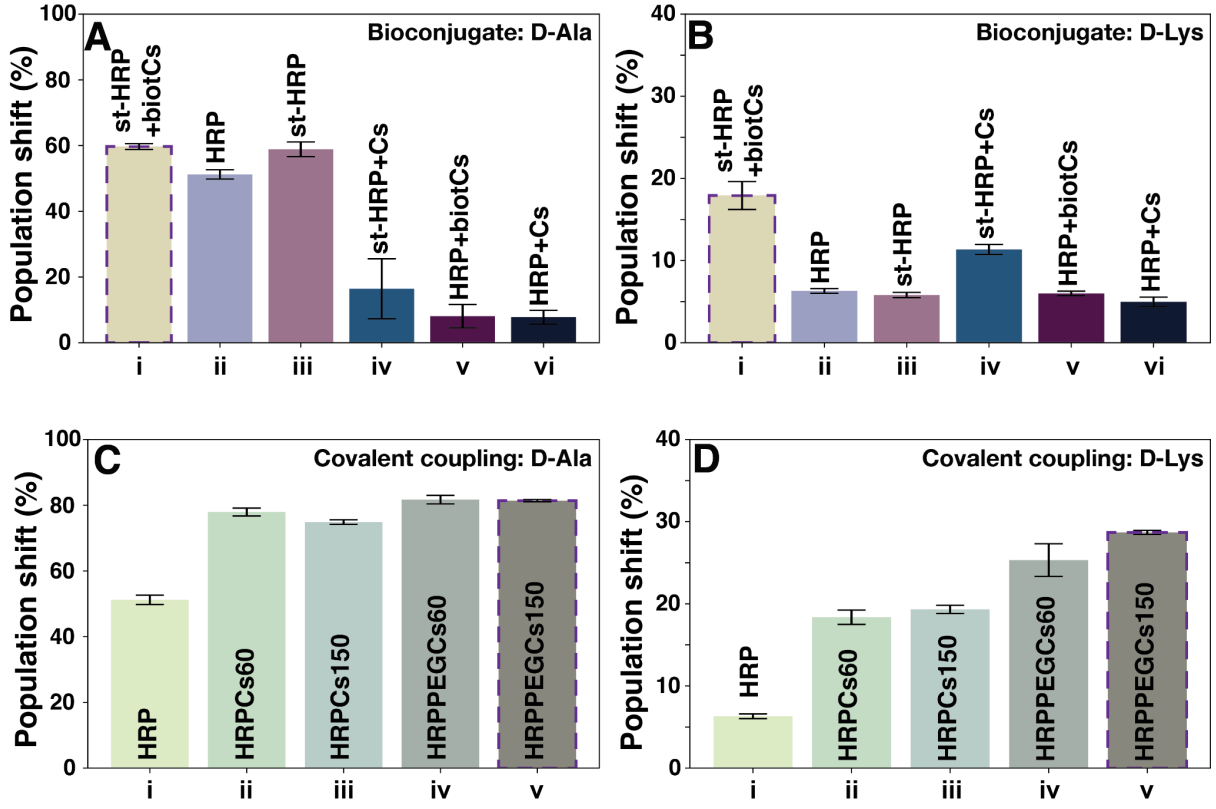

Figure 4: Bar graphs showing population shift (%) of the +/+ gate as a function of construct, as well as controls, for the bioconjugate approach with (A) D-Ala and (B) D-Lys as the substrates. Bar graphs showing population shift (%) of the +/+ gate as a function of construct, as well as controls, for both the carboxyl and cysteine coupling approaches with (C) D-Ala and (D) D-Lys as the substrates. In all cases n=3.

3.2.2 Carboxyl coupling of HRP to chitosan

Carboxyl coupling of HRP to Cs chains likely results in a heterogeneous mixture of attachment points on HRP. If residues within the enzyme's active site are involved, this could reduce enzyme activity. However, when conducting the labeling assay with HRP-Cs60 instead of the st-HRP+biot-Cs and utilizing both D-Ala and D-Lys as substrates, we observed high labeling efficiency. Specifically, we achieved up to 80% population labeling for D-Ala and approximately 20% for D-Lys (Figure 4C,ii and 4D,ii). This demonstrates an almost 30% increase compared to the corresponding control experiment using 45 μM of free HRP for D-Ala and a 4-fold increase for D-Lys.We further considered how the length of the Cs chain may impact the outcome of the labeling study. We hypothesized that longer chain lengths would permit functionalization of Cs with more HRPs per chain, thus increasing the

labeling efficiency. This was only partially validated by mass photometry, likely due to the chain degradation described above. Thus, in the case of the carboxyl coupling approach, no significant difference in labeling efficiency was observed for either D-Ala or D-Lys when HRP-Cs150 was used in place of HRP-Cs60 (Figure 4C,ii, 4C,iii, 4Dii, and 4D,iii)

3.2.2 Cysteine coupling of HRP to chitosan

Due to the substantial enhancement in labeling efficiency observed with the HRP-Cs constructs compared to the physically immobilized st-HRP/biot-Cs, we explored whether cysteine-coupled constructs would yield additional improvements. We based this assumption on two factors: firstly, the inclusion of the 5 kDa PEG linker used to tether the HRP to the Cs chain providing more freedom of movement to the auxiliary enzyme, and secondly, the more specific coupling strategy employed in this procedure. Similar to findings observed with carboxyl-coupled HRP-Cs constructs, the length of the chitosan had no significant impact on the efficiency of the labeling assay for D-Ala, while in the experiment performed with D-Lys, the use of a higher molecular weight chitosan (Cs150) resulted in a slight increase in the labeling signal (Figure 4C,iv, 4C,v, 4D,iv and 4D,v). The tyramide labeling reactions using D-Ala substrate and HRP constructs, HRP-PEG-Cs60 and HRP-PEG-Cs150, yielded similar outcomes, labeling around 80% of the *Rg*DAOx expressing cell population. This represents a signal enhancement of over 30% compared to the free HRP control and nearly 20% compared to the physically immobilized construct (Figure 4C,iv, 4C,v and 4A,i). However, it was only marginally more efficient, approximately 1-2%, than the HRP-Cs constructs. When testing the labeling reaction with D-Lys, the presence of HRP-PEG-Cs60 construct in the mixture led to a labeling of almost 25% of the yeast population, while in the case of HRP-PEG-Cs150 of almost 30% of the population, essentially improving the outcome of the assay by almost 4-fold in comparison to free HRP reaction control (Figure 4D,iv and 4D,v). This is a notable improvement over both the st-HRP+biot-Cs conjugate (Figure 4B,i) and the HRP-Cs60 and HRP-Cs-150 constructs (Figure 4D,ii and 4D,iii), which all show an increase of just over 2-fold compared to the HRP control. Analyzing the proposed chemical structure (Figure 2C) and the outcomes of the mass photometry investigation (Supplementary Figure S2), this increase in effectiveness for the low activity D-Lys with the HRP-PEG-Cs150, compared to the lower molecular weight HRP-PEG-Cs60 construct and the HRP-Cs constructs with no PEG spacer, is likely due to a combination of factors. These factors being the increased accessibility of the HRP due to the PEG spacer, and the presence of both singly and doubly HRP-functionalized Cs chains in the HRP-PEG-Cs150 construct (Supplementary Figure S2C), increasing the activity of the enzyme in close proximity to the cell surface.

Finally, to ensure that the improvements in labeling efficiency observed using the HRP-PEG-Cs150 and D-Ala were mainly due to charge interactions between the conjugated chitosan and surface of the yeast, rather than to a simple change in viscosity caused by the addition of the polysaccharide to the reaction mixture we compared the tyramide labeling experiment with a control reaction using free HRP in the presence of a 20 wt.% solution of PEG3350 as a viscosity enhancer (Supplementary Figure S7). In both cases, i.e., with D-Lys and D-Ala as substrates, the addition of PEG improves the outcome of the labeling reaction compared to the free HRP control. This validates previous observations that viscosity hinders diffusion and improves labeling efficiency. However, in the case of both substrates, the HRP-PEG-Cs150 provides a further noticeable improvement over both the free HRP and

HRP/PEG labeling solutions. This led to the conclusion that labeling efficiency can be more effectively improved through targeted interactions between reaction intermediates and the cell surface than simply increasing solution viscosity to hinder diffusion in the reaction.

3.3 Exploring labeling outcomes across reaction rates

Our optimization process involved comparing labeling assay outcomes using D-Ala, processed by *Rg*DAOx at a high turnover rate, and D-Lys, converted at a much lower rate. We demonstrated that compared to a standard homogeneous liquid-phase labeling reactions with soluble HRP, the cysteine coupled chitosan construct (HRP-PEG-Cs150) resulted in a 0.6-fold increase in yeast population labeling for D-Ala and a 3.5-fold increase for D-Lys. To further assess the performance of the optimized system across a wider range of reaction speeds, we extended our study to include the labeling of yeast using a broader substrate range. We first performed an Amplex Red activity assay to evaluate the reaction rate of *Rg*DAOx in the presence of 18 D-amino acids (all D-amino acids, except D-aspartic acid). From the outcomes of this assay we classified the substrates into groups of high, medium, and low turnover rate. We chose 9 substrates from these categories for further testing of the labeling assay in the presence of HRP-PEG-Cs150. Specifically, D-Ala, D-Leu and D-Val were chosen as high speed substrates; D-Ser, D-Trp and D-Pro as substrates processed at medium speed and D-Lys, D-His and D-Arg as low speed substrates (Supplementary Figure S4).

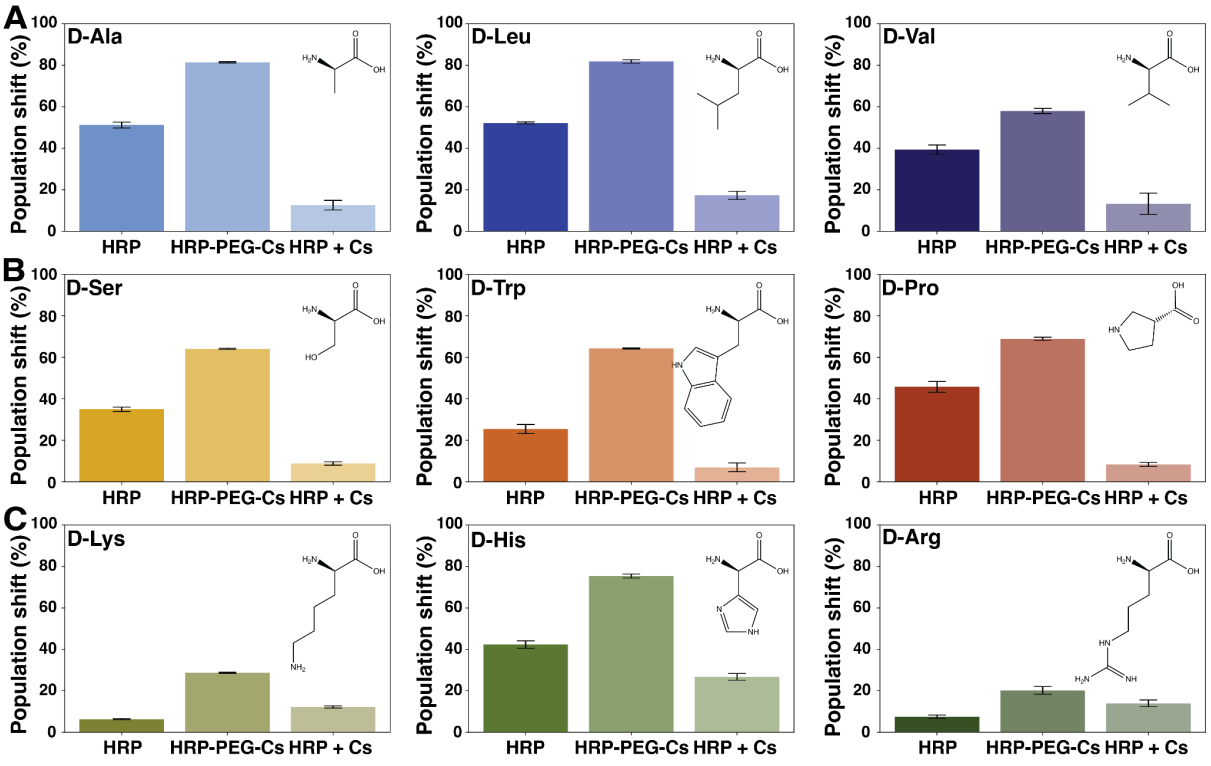

Figure 5: Bar graphs showing tyramide assay population shift (%) in the +/+ gate as a function of free HRP, HRP-PEG-Cs and free HRP with unmodified Cs for high turnover substrates (A) D-Ala, D-Leu and D-Val, medium turnover substrates (B) D-Ser, D-Trp, D-Pro and low turnover substrates (C) D-Lys, D-His, and D-Arg.

The labeling assay with HRP-PEG-Cs150 and various substrates were compared to reactions conducted with free HRP, as well as with free HRP in the presence of unmodified Cs. This additional control was implemented to confirm that immobilization is indeed necessary for higher efficiency labeling, rather than solely the presence of both HRP and chitosan in solution.

Figure 5A illustrates the comparison of labeling signals induced by three high turnover substrates, D-Ala, D-Leu, and D-Val, using HRP-PEG-Cs150 in the tyramide reaction mixture. We achieved a labeling efficiency of almost 82% for both D-Ala and D-Leu, while nearly 60% of the *Rg*DAOx expressing cells were labeled with D-Val. Compared to the free HRP control, these labeling efficiencies represent improvements of 0.6-fold, 0.6-fold, and 0.5-fold for D-Ala, D-Leu, and D-Val, respectively. In all cases, both the free HRP reaction and the investigated construct outperform the free HRP and unconjugated Cs control.

For the medium activity substrates, D-Ser, D-Trp, and D-Pro (Figure 5B), the total portion of labeled cells in the presence of HRP-PEG-Cs150 was relatively similar, at 64%, 64%, and 69%, respectively. However, this represented a significant increase compared to the free HRP control, with enhancements of 0.8-fold, 1.5-fold, and 0.5-fold, respectively. Similar to the high turnover substrates, the effect of free HRP and unconjugated Cs in the labeling reaction was substantially lower compared to the other two tested conditions.

Finally, in Figure 5C, population shifts for substrates processed at a low turnover rate by *Rg*DAOx are shown. We observed 28.7%, 75.4%, and 20.2% labeling of *Rg*DAOx expressing cells when the assay was performed in the presence of D-Lys, D-His, and D-Arg, respectively, using the HRP-PEG-Cs150 construct. These represented increases in labeling efficiencies of 3.5-fold, 0.8-fold, and 1.7-fold compared to the tyramide reaction performed with free HRP. In the tyramide labeling assay conducted using *Rg*DAOx expressing cells and positively charged D-amino acids such as D-Lys, D-Arg, and D-His, achieving a detectable labeling signal typically demands several hours of incubation time in the presence of free HRP. The need for prolonged incubation is attributed to their low turnover rate and the tendency for reactants to diffuse away from the cell surface before sufficient H_2O_2 is generated. However, the significant improvements in labeling efficiency observed within just 1 hour of incubation in the presence of HRP-PEG-Cs150 suggest that localizing HRP at the cell surface could further enhance labeling efficiency without requiring extended incubation times, even for these substrates.

Performing the labeling reactions with both the HRP-PEG-Cs150 construct alongside a mixture of free HRP and unfunctionalized Cs facilitated investigation of the need for conjugation of the HRP to Cs across a range of substrates. In all cases, the labeling assay performed with HRP and unconjugated chitosan underperforms compared to the main reaction and free HRP control. We believe this might be due to the affinity of the positively charged Cs for the yeast cell surface, as schematically illustrated in Supplementary Figure S8A and S8B. When HRP is conjugated to the Cs, the HRP is maintained in close proximity to the surface displayed *Rg*DAOx permitting effective labeling (Supplementary Figure S8A). However, if the HRP is not tethered, the Cs forms a closely packed arrangement of chains over the cell surface that prevent the HRP from coming in contact with the *Rg*DAOx (Supplementary Figure S8B). Thus, it is clear from the outcomes of the experiments that the presence of Cs only improves the experimental outcome if it is tethered to the HRP (Figure 5). The only exception to this is in the case of D-Lys and D-Arg, in which the free Cs/free

HRP mixture out performs the free HRP, by a small degree. As reported in the literature,[46] an interaction between these D-amino acids and the unconjugated chitosan may hold the substrates close to the cell surface leading to a higher localized concentration of substrate and faster production of H_2O_2, resulting in higher labeling signal compared to the reaction performed with just free HRP.

4. Conclusions

This study reports the design and characterization of enzyme-polysaccharide conjugates designed to improve the single cell labeling efficiency in tyramide/peroxidase proximity labeling methods to allow assaying low turnover rate reactions. Three constructs were examined, wherein HRP, the auxiliary enzyme responsible for linking the product of the main reaction to the labeling process of the cells, was: (1) bioconjugated to the chitosan through a streptavidin-biotin linkage, (2) bound to the chitosan through carboxyl coupling, and (3) specifically bound through cysteine coupling with a 5 kDa PEG spacer. The bioconjugate approach proved to be the least efficient, whereas cysteine coupling through a PEG spacer yielded the best outcomes in terms of percentage of labeled yeast population, particularly when assaying low turnover rate reactions. This enzyme-polysaccharide conjugate allows for the use of tyramide labeling assays across a range of enzymatic reaction velocities, resulting in high efficiency labeling outcomes at low auxiliary enzyme concentrations (e.g., HRP). This could be highly beneficial for single-cell labeling systems that require multi-enzyme cascades to link the main reaction product to cell labeling, especially considering that use of high auxiliary enzyme concentrations are often cost-prohibitive.

Author Contributions

M.H. curated data, conducted the formal analysis of the data, performed the laboratory investigations, validated and visualized the data. M.A.N acquired funding for the investigation and provided resources. R.V. and Z.W.K. conceptualized the study, curated data, developed methodologies, administered the project, supervised the development of the study, validated experiments, visualized data and wrote the original draft of the manuscript. Z.W.K also acquired funding for the study. All authors reviewed and edited the manuscript.

Conflicts of interest

There are no conflicts to declare

Acknowledgements

This work was supported by the University of Basel, ETH Zurich, the SNF-NCCR in Molecular Systems Engineering, and an SNSF Grant (200021_191962) to M.A.N. Z.W.K. would like to acknowledge funding from the European Union's Horizon 2020 research and innovation programme under the Marie Skłodowska-Curie grant agreement No. 842043.

References

(1) Romero, P. A.; Arnold, F. H. Exploring Protein Fitness Landscapes by Directed Evolution. *Nat. Rev. Mol. Cell Biol.* **2009**, *10*, 866.
(2) Starita, L. M.; Fields, S. Deep Mutational Scanning: A Highly Parallel Method to Measure the Effects of Mutation on Protein Function. *Cold Spring Harb. Protoc.* **2015**, *2015* (8), 711–714.
(3) Fowler, D. M.; Fields, S. Deep Mutational Scanning: A New Style of Protein Science. *Nat.*

Methods **2014**, *11* (8), 801–807.
(4) Vanella, R.; Kovacevic, G.; Doffini, V.; de Santaella, J. F.; Nash, M. A. High-Throughput Screening, next Generation Sequencing and Machine Learning: Advanced Methods in Enzyme Engineering. *Chem. Commun.* **2022**, *58* (15), 2455–2467.
(5) Agresti, J. J.; Antipov, E.; Abate, A. R.; Ahn, K.; Rowat, A. C.; Baret, J.-C.; Marquez, M.; Klibanov, A. M.; Griffiths, A. D.; Weitz, D. A. Ultrahigh-Throughput Screening in Drop-Based Microfluidics for Directed Evolution. *Proc. Natl. Acad. Sci. U. S. A.* **2010**, *107* (9), 4004–4009.
(6) Vanella, R.; Ta, D. T.; Nash, M. A. Enzyme-mediated Hydrogel Encapsulation of Single Cells for High-throughput Screening and Directed Evolution of Oxidoreductases. *BioTechnology* **2019**.
(7) Ding, M.; Clark, R.; Bardelle, C.; Backmark, A.; Norris, T.; Williams, W.; Wigglesworth, M.; Howes, R. Application of High-Throughput Flow Cytometry in Early Drug Discovery: An AstraZeneca Perspective. *SLAS Discov* **2018**, *23* (7), 719–731.
(8) Stucki, A.; Vallapurackal, J.; Ward, T. R.; Dittrich, P. S. Droplet Microfluidics and Directed Evolution of Enzymes: An Intertwined Journey. *Angew. Chem. Int. Ed Engl.* **2021**, *60* (46), 24368–24387.
(9) Matsumoto, A. Development of Heat-Responsive Adhesive Materials That Are Stable during Use and Quickly Deteriorate during Dismantling. *Polym. J.* **2023**, *56* (4), 223–247.
(10) Gantz, M.; Neun, S.; Medcalf, E. J.; van Vliet, L. D.; Hollfelder, F. Ultrahigh-Throughput Enzyme Engineering and Discovery in In Vitro Compartments. *Chem. Rev.* **2023**, *123* (9), 5571–5611.
(11) Wang, Z.; Wang, H.; Lin, S.; Ahmed, S.; Angers, S.; Sargent, E. H.; Kelley, S. O. Nanoparticle Amplification Labeling for High-Performance Magnetic Cell Sorting. *Nano Letters* **2022**, *22* (12), 4774–4783.
(12) Porebski, B. T.; Balmforth, M.; Browne, G.; Riley, A.; Jamali, K.; Fürst, M. J. L. J.; Velic, M.; Buchanan, A.; Minter, R.; Vaughan, T.; Holliger, P. Rapid Discovery of High-Affinity Antibodies via Massively Parallel Sequencing, Ribosome Display and Affinity Screening. *Nature Biomedical Engineering* **2023**.
(13) Guo, J.; Guo, S.; Lu, S.; Gong, J.; Wang, L.; Ding, L.; Chen, Q.; Liu, W. The Development of Proximity Labeling Technology and Its Applications in Mammals, Plants, and Microorganisms. *Cell Commun. Signal.* **2023**, *21* (1), 1–22.
(14) Qin, W.; Cho, K. F.; Cavanagh, P. E.; Ting, A. Y. Deciphering Molecular Interactions by Proximity Labeling. *Nat. Methods* **2021**, *18* (2), 133–143.
(15) Vanella, R.; Bazin, A.; Ta, D. T.; Nash, M. A. Genetically Encoded Stimuli-Responsive Cytoprotective Hydrogel Capsules for Single Cells Provide Novel Genotype–Phenotype Linkage. *Chem. Mater.* **2019**. https://doi.org/10.1021/acs.chemmater.8b04348.
(16) Küng, C.; Vanella, R.; Nash, M. A. Directed Evolution of Rhodotorula Gracilisd-Amino Acid Oxidase Using Single-Cell Hydrogel Encapsulation and Ultrahigh-Throughput Screening. *React Chem Eng* **2023**, *8* (8), 1960–1968.
(17) Fernández De Santaella, J.; Ren, J.; Vanella, R.; Nash, M. A. Enzyme Cascade with Horseradish Peroxidase Readout for High-Throughput Screening and Engineering of Human Arginase-1. *Anal. Chem.* **2023**, *95* (18), 7150–7157.
(18) Hung, V.; Udeshi, N. D.; Lam, S. S.; Loh, K. H.; Cox, K. J.; Pedram, K.; Carr, S. A.; Ting, A. Y. Spatially Resolved Proteomic Mapping in Living Cells with the Engineered Peroxidase APEX2. *Nature Protocols* **2016**, *11*, 456–475.
(19) Singer-Krüger, B.; Fröhlich, T.; Franz-Wachtel, M.; Nalpas, N.; Macek, B.; Jansen, R.-P. APEX2-Mediated Proximity Labeling Resolves Protein Networks in Saccharomyces Cerevisiae Cells. *FEBS J.* **2020**, *287* (2), 325–344.
(20) Cisneros, B. T.; Devaraj, N. K. Laccase-Mediated Catalyzed Fluorescent Reporter Deposition for Live-Cell Imaging. *Chembiochem* **2020**, *21* (1-2), 98–102.
(21) Roberts, J. J.; Naudiyal, P.; Lim, K. S.; Poole-Warren, L. A.; Martens, P. J. A Comparative Study of Enzyme Initiators for Crosslinking Phenol-Functionalized Hydrogels for Cell Encapsulation. *Biomaterials Research* **2016**, *20* (1), 1–12.
(22) Vanella, R.; Küng, C.; Schoepfer, A. A.; Doffini, V.; Ren, J.; Nash, M. A. Understanding Activity-Stability Tradeoffs in Biocatalysts by Enzyme Proximity Sequencing. *Nature Communications* **2024**, *15*, 1807.
(23) Walsh, Z.; Janeček, E.-R.; Hodgkinson, J. T.; Sedlmair, J.; Koutsioubas, A.; Spring, D. R.; Welch, M.; Hirschmugl, C. J.; Toprakcioglu, C.; Nitschke, J. R.; Jones, M.; Scherman, O. A. Multifunctional Supramolecular Polymer Networks as next-Generation Consolidants for Archaeological Wood Conservation. *Proc. Natl. Acad. Sci. U. S. A.* **2014**, *111* (50), 17743–17748.
(24) Umhau, S.; Pollegioni, L.; Molla, G.; Diederichs, K.; Welte, W.; Pilone, M. S.; Ghisla, S. The X-Ray Structure of D-Amino Acid Oxidase at Very High Resolution Identifies the Chemical

Mechanism of Flavin-Dependent Substrate Dehydrogenation. *Proc. Natl. Acad. Sci. U. S. A.* **2000**, *97* (23), 12463–12468.
(25) Pollegioni, L.; Falbo, A.; Pilone, M. S. Specificity and Kinetics of Rhodotorula Gracillisd-Amino Acid Oxidase. *Biochimica et Biophysica Acta (BBA) - Protein Structure and Molecular Enzymology* **1992**, *1120* (1), 11–16.
(26) Pollegioni, L.; Diederichs, K.; Molla, G.; Umhau, S.; Welte, W.; Ghisla, S.; Pilone, M. S. Yeast D-Amino Acid Oxidase: Structural Basis of Its Catalytic Properties. *J. Mol. Biol.* **2002**, *324* (3), 535–546.
(27) Pilone, M. S. D-Amino Acid Oxidase: New Findings. *Cell. Mol. Life Sci.* **2000**, *57* (12), 1732–1747.
(28) Heiniger, M. Optimization of Single Cell Tyramide/peroxidase Labelling Assay by Polysaccharide Encapsulation. M.Sc., University of Basel, 2023.
(29) Ma, P. L.; Lavertu, M.; Winnik, F. M.; Buschmann, M. D. New Insights into Chitosan-DNA Interactions Using Isothermal Titration Microcalorimetry. *Biomacromolecules* **2009**, *10* (6), 1490–1499.
(30) Tan, S.; Gu, D.; Liu, H.; Liu, Q. Detection of a Single Enzyme Molecule Based on a Solid-State Nanopore Sensor. *Nanotechnology* **2016**, *27* (15), 155502.
(31) Chirra, H. D.; Sexton, T.; Biswal, D.; Hersh, L. B.; Hilt, J. Z. Catalase-Coupled Gold Nanoparticles: Comparison between the Carbodiimide and Biotin-Streptavidin Methods. *Acta Biomater.* **2011**, *7* (7), 2865–2872.
(32) Berglund, G. I.; Carlsson, G. H.; Smith, A. T.; Szöke, H.; Henriksen, A.; Hajdu, J. The Catalytic Pathway of Horseradish Peroxidase at High Resolution. *Nature* **2002**, *417* (6887), 463–468.
(33) Krissinel, E.; Henrick, K. Detection of Protein Assemblies in Crystals. In *Computational Life Sciences*; Springer Berlin Heidelberg, 2005; pp 163–174.
(34) Krissinel, E.; Henrick, K. Inference of Macromolecular Assemblies from Crystalline State. *J. Mol. Biol.* **2007**, *372* (3), 774–797.
(35) Krissinel, E. Crystal Contacts as Nature's Docking Solutions. *J. Comput. Chem.* **2010**, *31* (1), 133–143.
(36) Katz, B. A.; Kossiakoff, A. The Crystallographically Determined Structures of Atypical Strained Disulfides Engineered into Subtilisin. *J. Biol. Chem.* **1986**, *261* (33), 15480–15485.
(37) Aranaz, I.; Alcántara, A. R.; Civera, M. C.; Arias, C.; Elorza, B.; Heras Caballero, A.; Acosta, N. Chitosan: An Overview of Its Properties and Applications. *Polymers* **2021**, *13* (19). https://doi.org/10.3390/polym13193256.
(38) Huang, H.; Yuan, Q.; Yang, X. Preparation and Characterization of Metal-Chitosan Nanocomposites. *Colloids Surf. B Biointerfaces* **2004**, *39* (1-2), 31–37.
(39) Esumi, K.; Takei, N.; Yoshimura, T. Antioxidant-Potentiality of Gold–chitosan Nanocomposites. *Colloids Surf. B Biointerfaces* **2003**, *32* (2), 117–123.
(40) Jendryczko, K.; Rzeszotko, J.; Krzyscik, M. A.; Kocyła, A.; Szymczyk, J.; Otlewski, J.; Szlachcic, A. Drug Conjugation via Maleimide-Thiol Chemistry Does Not Affect Targeting Properties of Cysteine-Containing Anti-FGFR1 Peptibodies. *Mol. Pharm.* **2022**, *19* (5), 1422–1433.
(41) Young, G.; Hundt, N.; Cole, D.; Fineberg, A.; Andrecka, J.; Tyler, A.; Olerinyova, A.; Ansari, A.; Marklund, E. G.; Collier, M. P.; Chandler, S. A.; Tkachenko, O.; Allen, J.; Crispin, M.; Billington, N.; Takagi, Y.; Sellers, J. R.; Eichmann, C.; Selenko, P.; Frey, L.; Riek, R.; Galpin, M. R.; Struwe, W. B.; Benesch, J. L. P.; Kukura, P. Quantitative Mass Imaging of Single Biological Macromolecules. *Science* **2018**, *360* (6387), 423–427.
(42) den Boer, M. A.; Lai, S.-H.; Xue, X.; van Kampen, M. D.; Bleijlevens, B.; Heck, A. J. R. Comparative Analysis of Antibodies and Heavily Glycosylated Macromolecular Immune Complexes by Size-Exclusion Chromatography Multi-Angle Light Scattering, Native Charge Detection Mass Spectrometry, and Mass Photometry. *Anal. Chem.* **2022**, *94* (2), 892–900.
(43) Cramer, D. A. T.; Franc, V.; Heidenreich, A.-K.; Hook, M.; Adibzadeh, M.; Reusch, D.; Heck, A. J. R.; Haberger, M. Characterization of High-Molecular Weight by-Products in the Production of a Trivalent Bispecific 2+1 Heterodimeric Antibody. *MAbs* **2023**, *15* (1), 2175312.
(44) Houen, G.; Hansen, K. Interference of Sugars with the Binding of Biotin to Streptavidin and Avidin. *J. Immunol. Methods* **1997**, *210* (2), 115–123.
(45) Hirayama, H.; Matsuda, T.; Tsuchiya, Y.; Oka, R.; Seino, J.; Huang, C.; Nakajima, K.; Noda, Y.; Shichino, Y.; Iwasaki, S.; Suzuki, T. Free Glycans Derived from O-Mannosylated Glycoproteins Suggest the Presence of an O-Glycoprotein Degradation Pathway in Yeast. *J. Biol. Chem.* **2019**, *294* (44), 15900–15911.
(46) Ibrahim, M. A.; Gawad, A. E.-D. A. Spectroscopic Analyses of Chitosan Interactions with Amino Acids. *J. Comput. Theor. Nanosci.* **2012**, *9* (8), 1120–1124.

Supplementary Information

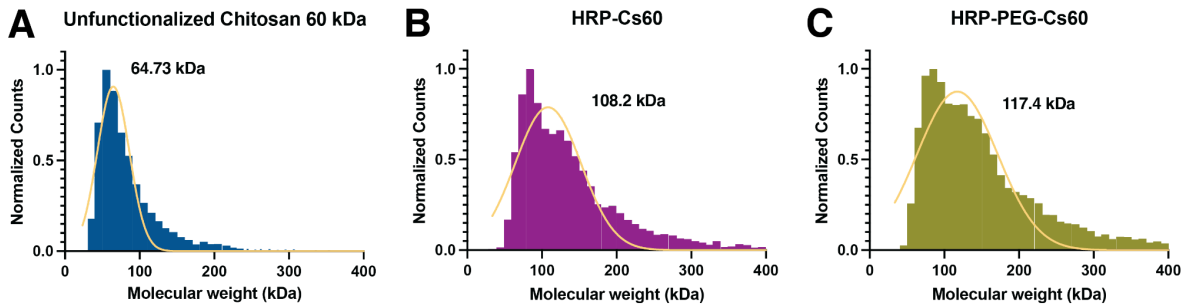

Figure S1: Mass photometry results showing unfunctionalized 60 kDa chitosan (A), HRP-functionalized 60 kDa Cs (B), and HRP-PEG-functionalized 60 kDa Cs (C).

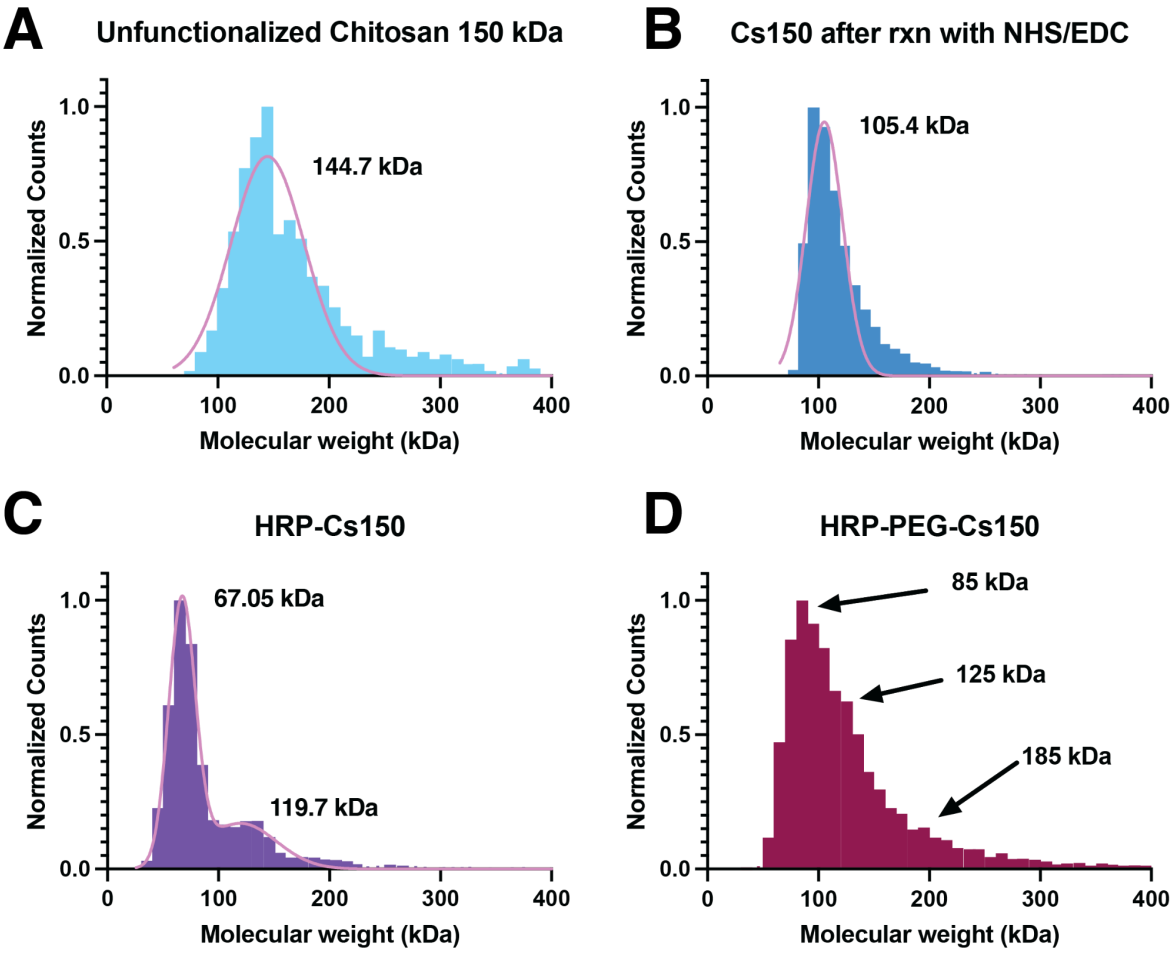

Figure S2: Mass photometry results showing unfunctionalized 150 kDa chitosan (A) and after 1 h reaction in the presence of NHS/EDC required for the functionalization (B), HRP-functionalized 150 kDa Cs (C), and HRP-PEG-functionalized 150 kDa Cs (D).

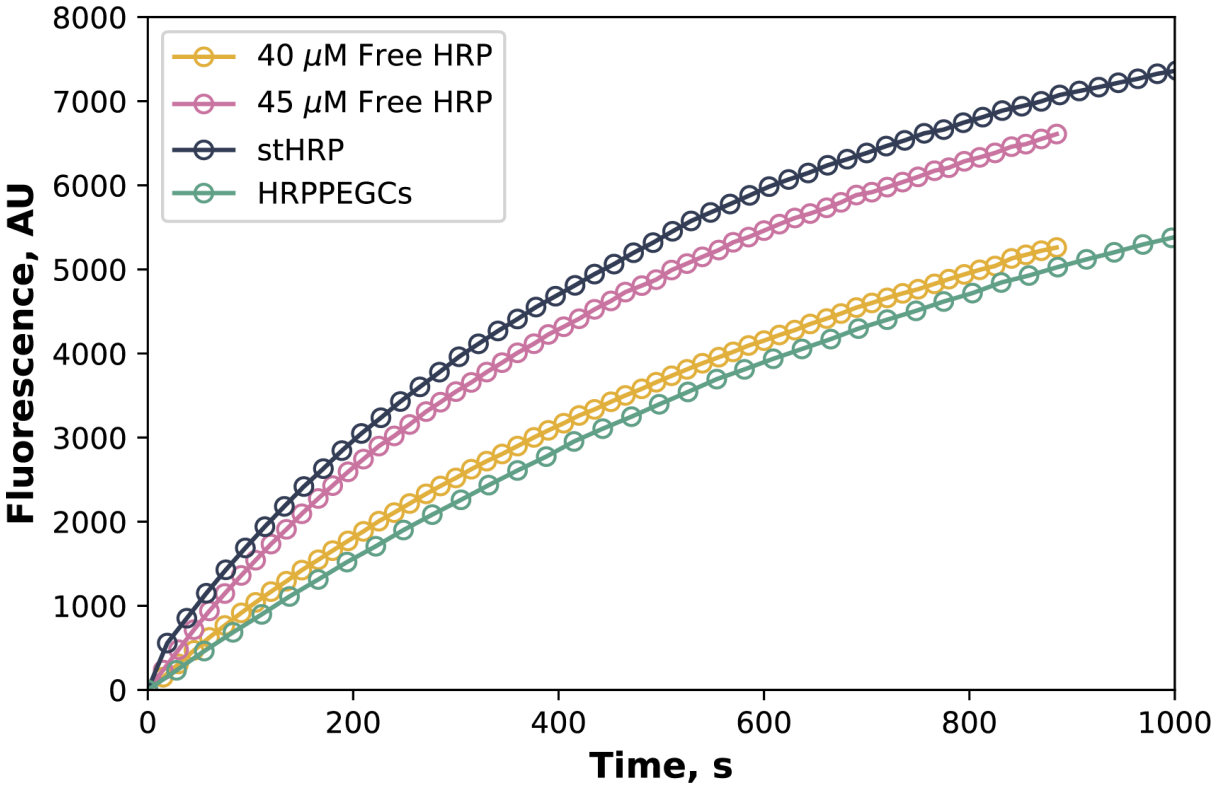

Figure S3: Amplex Red activity assay comparing the activity of 1 μM st-HRP, a 1.6 wt.% solution of HRP-PEG-Cs, and two concentrations of free HRP in solution (40 and 45 μM).

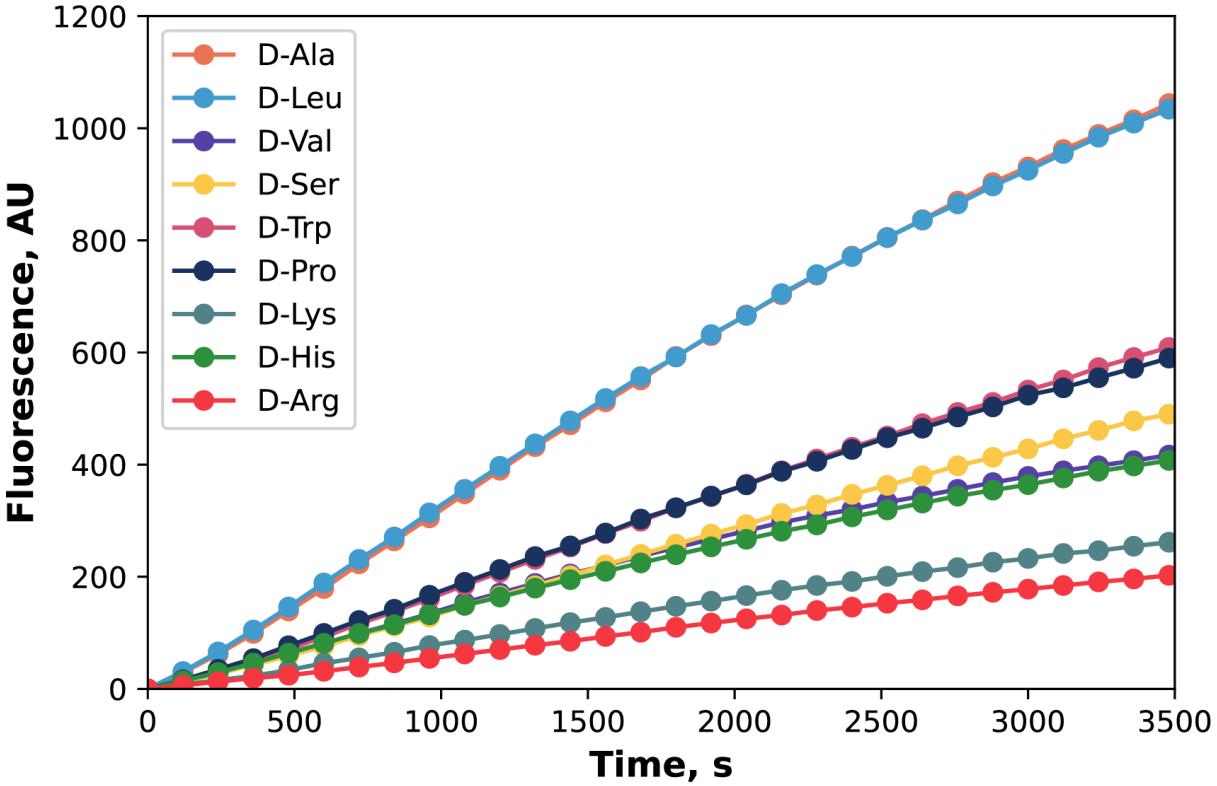

Figure S4: Amplex Red activity assay comparing the relative activity of surface displayed *Rg*DAOx for each of the 9 chosen D amino acid substrates at the concentrations reported in Table 2 and in presence of 45 μM soluble HRP.

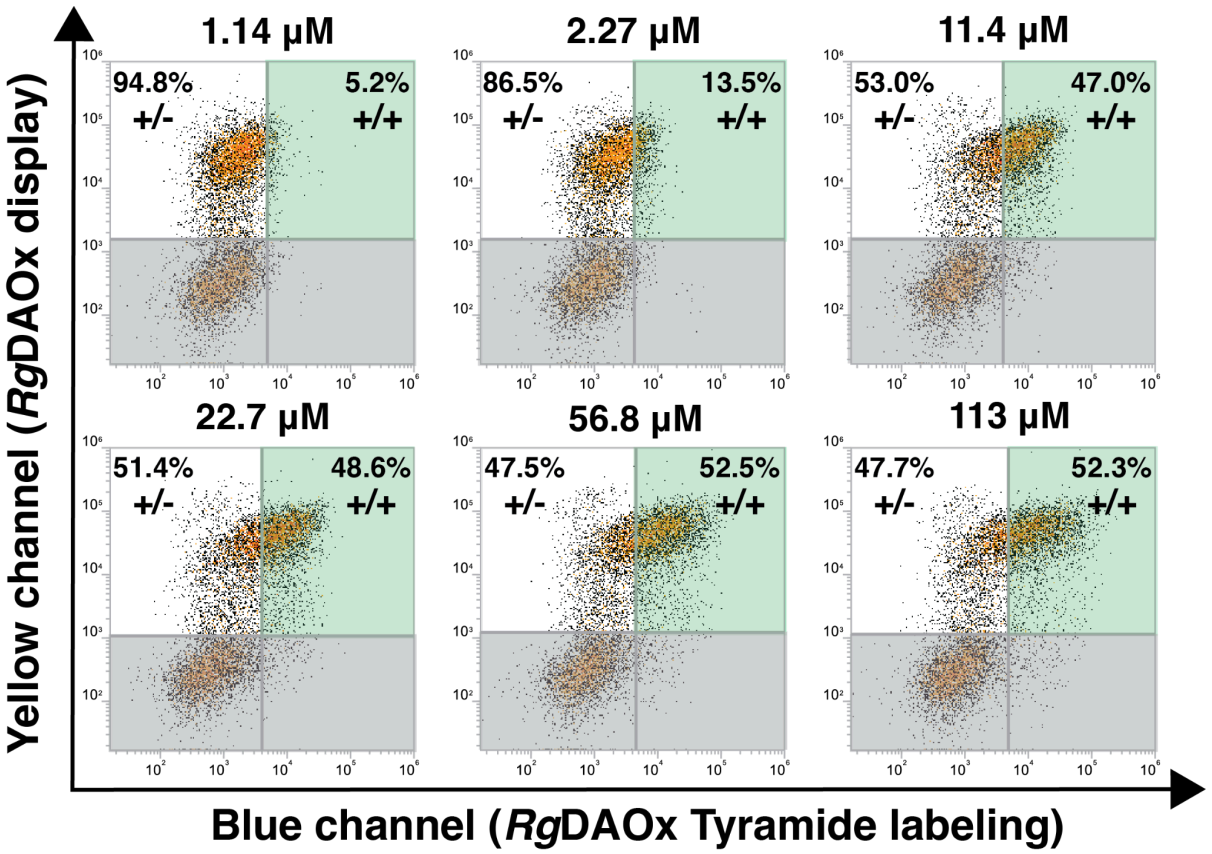

Figure S5: Flow cytometry analyses of tyramide labeling assays of yeast cells displaying *Rg*DAOx in presence of free HRP at varying concentrations and D-Ala as substrate (n = 3)

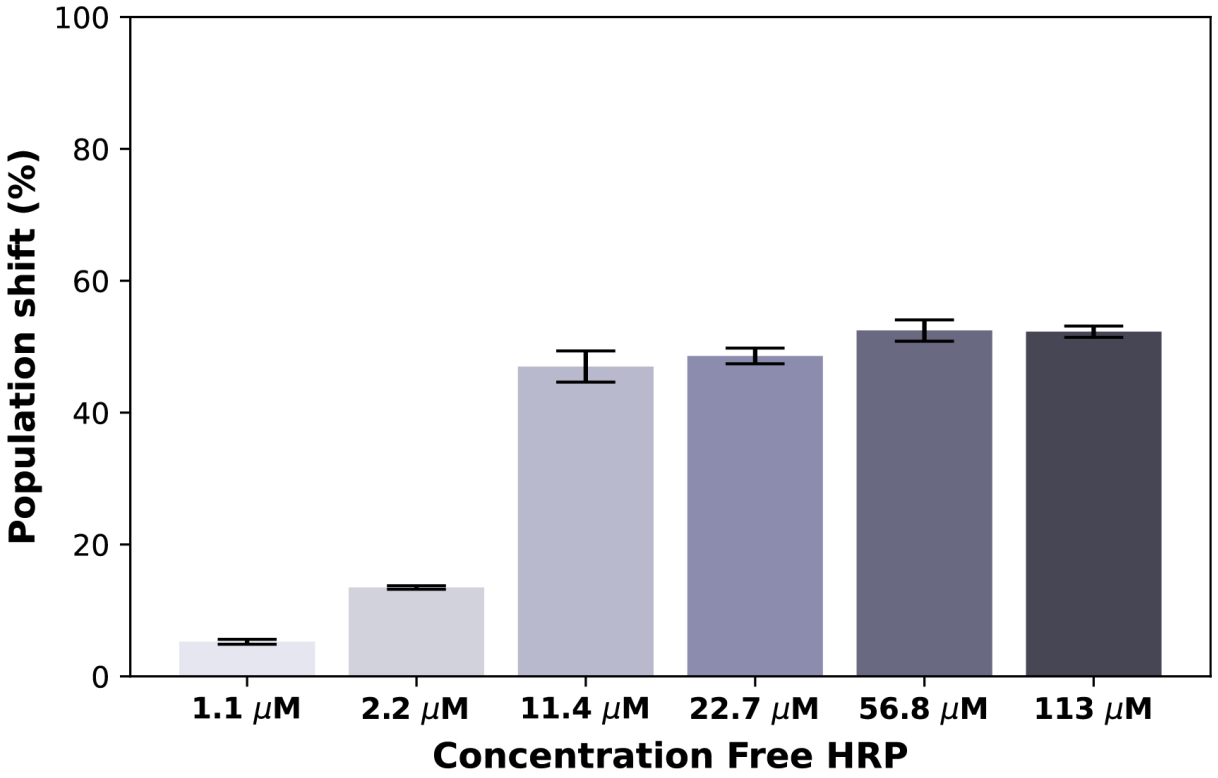

Figure S6: Bar graph showing the percentage population shift within the +/+ gate after the tyramide labeling reaction. The experiment was conducted using yeast cells expressing wild-type *Rg*DAOx and different concentrations of free HRP, ranging from 1.14 to 113 μM. The substrate employed for the reaction was D-Ala.

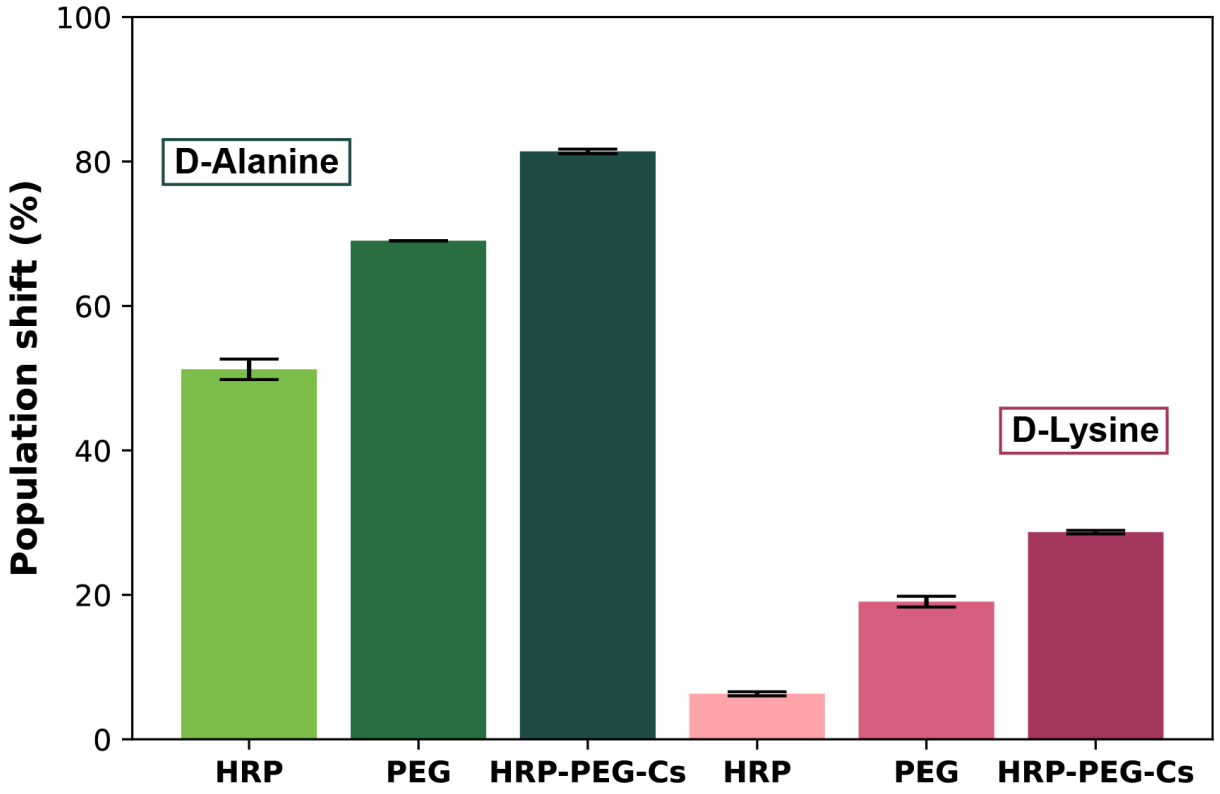

Figure S7: Bar graph displaying the percentage population shift within the +/+ gate after the tyramide labeling reaction. The experiment involved yeast cells expressing wild-type *Rg*DAOx with D-Ala (green) and D-Lys (pink) substrates. Free HRP at 45 μM, free HRP and 20% w/v of PEG3350 and HRP-PEG-Cs150 solutions were used, respectively.

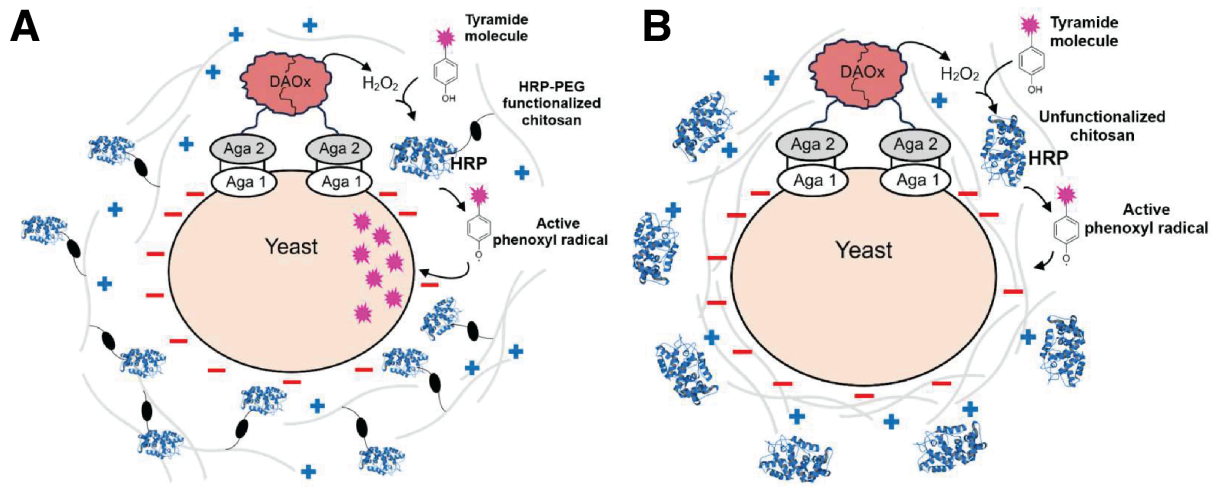

Figure S8: Graphical illustration depicting the behavior of the tyramide labeling system under two conditions: (A) When HRP is covalently bound to the chitosan chains, thereby recruited to the cell through charge interaction of the polysaccharide with the yeast surface. (B) When both HRP and unconjugated chitosan are free in solution, and chitosan surrounds the cell surface through charge interaction, excluding the HRP from approaching the yeast surface.